Local structure anomaly with the charge ordering transition of $1T$-TaS_2

Sharon S. Philip,[1] Joerg C. Neuefeind,[2] Matthew B. Stone,[2] and Despina Louca[1,*]
[1]*Department of Physics, University of Virginia, Charlottesville, Virginia 22904, USA*
[2]*Oak Ridge National Laboratory, Oak Ridge, Tennessee 37830, USA*

(Received 8 November 2022; revised 4 March 2023; accepted 25 April 2023; published 15 May 2023)

The quasi-two-dimensional $1T$-TaS_2 displays a unique two-step charge density wave (CDW) transition, from incommensurate (ICDW) to nearly commensurate (NCDW), and from NCDW to commensurate (CCDW), which is reflected in the stepwise resistivity behavior. In this work, we show that the hysteresis observed in the resistivity across the NCDW-to-CCDW transition is coupled to a local structure anomaly, evident from the pair density function analysis of neutron and x-ray diffraction data. We find that upon cycling the system from high to low temperatures (through the NCDW-CCDW transition) and collecting data on warming, local distortions in the in-star Ta and out-of-plane S atoms become evident, disrupting the trigonal symmetry of the star of David structures, without breaking the lattice periodicity, and preserving the underlying $P\bar{3}$ symmetry. When the system is warmed up from the NCDW to the ICDW state, the local distortions are absent and the stars are symmetric, indicating that it is the thermal cycling through the NCDW-CCDW that locks in the distortions. Furthermore, we verify the temperature dependence of the two types of stacking along the c axis: at low temperatures, the layer stacking exhibits a $13c_o$ order that disappears upon warming through the NCDW transition, while across the NCDW and ICDW phases, the layer stacking is $3c_o$. The $3c_o$ order gradually disappears in the ICDW state.

DOI: 10.1103/PhysRevB.107.184109

Charge density waves (CDW) are electronic instabilities that propagate through the lattice and often drive the system to a new crystal periodicity as they spontaneously break the symmetry [1]. The new superlattice modulations introduce a gap in the electron density of states. The mechanism behind this phenomenon, however, has been a subject of ongoing debate, especially in the quasi-two-dimensional (2D) transition metal dichalcogenides (TMDs) $1T$-MX_2 (M = Ti, Ta and X = S, Se, Te) [2–9]. Several scenarios have been proposed to explain the origin of the gap that include band filling due to layer pairing, electron-phonon coupling, or electron-electron correlations leading to a Mott state [3,10–15]. Given their layered nature, the out-of-plane coupling is important to understand the electronic characteristics of these materials, with band structure calculations having shown that opening a gap at the Γ point depends on the orbital order and out-of-plane stacking [16,17]. Moreover, density functional theory (DFT) predicts that the metal-insulator transition (MIT) arises not from the in-plane superstructure but from the out-of-plane ordering of the superstructure [18]. To this end, the temperature dependence of the crystal structure of $1T$-TaS_2 is essential and is investigated by combining single crystal x-ray diffraction with the local structure analysis of neutron powder diffraction.

TMDs are fertile ground for probing coexisting and/or competing nontrivial quantum effects arising from CDW order [3,19], superconductivity [20–25] and possibly a quantum spin liquid (QSL) [26–31]. Although a model system to study many-body electron and phonon interactions, TMDs are exploited for engineering applications [4] and exhibit a multitude of phase transitions and crossovers between proximate states upon cooling, chemical doping [32,33], layer stacking, applied strain, or pressure [4,6,34–40]. Such is the case for $1T$-TaS_2 with the crystal structure shown in Fig. 1(a), where the compound is a host of multiple CDW transitions [3,41]. Although not superconducting at ambient conditions, superconductivity appears in $1T$-TaS_2 under pressure or when doped with selenium (Se) [42–44].

$1T$-TaS_2 undergoes a unique transformation from the high-temperature crystal phase to a commensurate CDW state that can potentially lead to a quantum triangular antiferromagnet (AFM) [see Fig. 1(a)]. Such an AFM state has not been observed thus far. The CDW order is accompanied by periodic lattice distortions that effectively change the long-range order and can be measured by diffraction techniques. Upon cooling, $1T$-TaS_2 exhibits three CDW transitions: At very high temperatures, the trigonal structure with $P\bar{3}m1$ symmetry [Fig. 1(b)] goes through an ICDW phase around $T_{\mathrm{ICDW}} \sim 540$ K due to a Fermi surface instability [45]. Further cooling leads to a transition from the ICDW to NCDW at $T \sim 350$ K, at which point the $\sqrt{13}a\,\sqrt{13}a$ structural modulation first appears with $\sim 12^\circ$ tilt relative to the ab plane. Below 180 K, the $\sqrt{13}a\,\sqrt{13}a$ structural modulation changes to a rotation of 13.9° relative to the plane and the CDW becomes commensurate [see the commensurate lattice comprising six pointed stars of David in Fig. 1(a)]. The star formation results when 12 Ta atoms move towards the central Ta atom [2,41,46]. As shown previously, the CDW transitions coincide with distinct kinks in the transport [shown in Fig. 1(d)] [3,42]. On cooling below 350 K, a jump is observed in the resistivity. This temperature corresponds to the ICDW-NCDW transition. Upon further cooling, a second jump is observed around 180 K, which corresponds

*Corresponding author: louca@virginia.edu

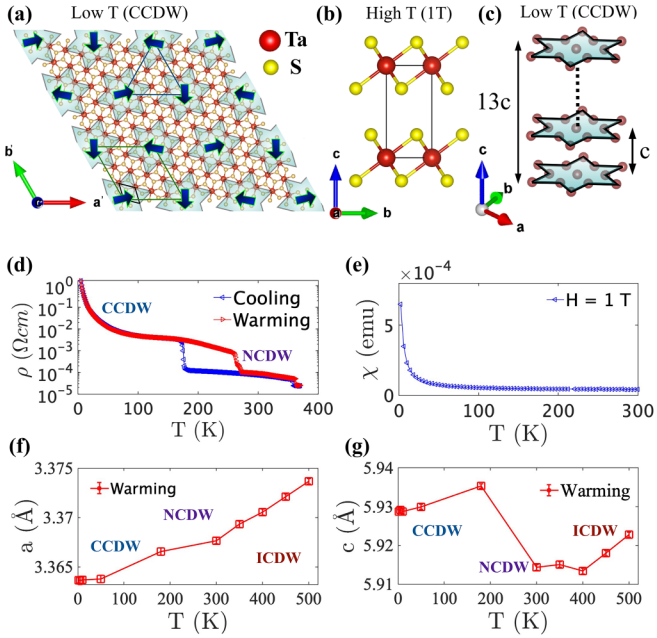

FIG. 1. (a) Schematic diagram of the $\sqrt{13}a \cdot \sqrt{13}a$ supercell in the CCDW phase. Stars of David are colored green. The uncompensated Ta spin, $S = 1/2$, is shown by blue arrows at the center of the stars. The $1T$ unit cell and superlattice unit cell are marked by a small black and a large green rhombus, respectively. (b) The high temperature unit cell with the $P\bar{3}m1$ symmetry of the $1T$ phase. (c) The low temperature unit cell showing $13c$ stacking in CCDW phase. (d) The resistivity as a function of temperature on a single crystal sample in logarithmic scale. The multiple CDW phase transitions are seen in both cooling and warming. (e) The magnetic susceptibility as a function of temperature at an applied field of $1T$ and ambient pressure shows a paramagnetic response at low temperatures. (f) The in-plane lattice constant a as a function of temperature changes the slope around the NCDW-CCDW transition. (g) The c-lattice constant showing discontinuity around the CCDW-NCDW steps and at the NCDW-ICDW steps.

to the NCDW-CCDW transition. The resistivity curve continues to rise as the CCDW state becomes more insulating. The bulk susceptibility shown in Fig. 1(e) indicates that this system is paramagnetic down to the lowest temperature.

The SODs consists of 13 atoms with 12 Ta atoms at the vertices surrounding one lone Ta atom at the center responsible for half-filling of one of the bands. The 12 atom pairs form six occupied bands while the 13th atom is left with one unpaired spin in the $5d^1$-d_z^2 half-filled band [10,15,47]. The spin-$\frac{1}{2}$ resides on a triangular lattice shown in Fig. 1(a) that is inherently frustrated and quantum fluctuations prevent magnetic ordering down to the lowest temperature [27]. The half-filled band is nominally metallic, but it is evident from the resistivity that the system becomes insulating. Whether $1T$-TaS_2 is a Mott insulator or a band insulator has been highly debated in recent years because the insulating ground state can be explained in terms of out-of-plane stacking without needing to invoke electron correlations. In this work, we show that upon cycling the system from high to low temperatures, in-plane Ta distortions become evident due to faults in the SODs that locally break the trigonal symmetry but not globally. If, on the other hand, the system is not cooled down to low temperatures prior to measurement, the local distortions are absent. Coupled with the local distortions, we observe out-of-plane sulfur distortions just as in other studies [10,41] that exhibit the same thermal hysteresis as the Ta ions. Furthermore, the layer stacking order has been highly debated over the years. Here, we confirm that a $13c$ order is present at low temperatures that is replaced by a $3c$ layer stacking in going through the NCDW transition. The $13c$ layer stacking gradually disappears across the CCDW-NCDW transition while the $3c$ stacking order appears in the NCDW state and gradually dissipates across the ICDW phase. Powders and single crystals were prepared using solid-state reaction and chemical vapor transport, respectively. Synchrotron x-ray and neutron powder diffraction measurements were performed to investigate the structure through the multiple CDW steps. X-ray powder diffraction measurements were carried out at room temperature using the high-energy beamline (105.7 keV) at the 11-ID-C beamline at the Advanced Photon Source of Argonne National Laboratory. The time-of-flight (TOF) neutron measurements were carried out at the Nanoscale Ordered Materials Diffractometer (NOMAD/BL-1B) and SEQUOIA (BL-17), a direct geometry spectrometer, at the Spallation Neutron Source (SNS) of Oak Ridge National Laboratory (ORNL) at temperatures ranging from 2 to 500 K. The aluminium can was used for SEQUOIA measurements and the empty can data were subtracted from the data. The Vanadium empty can subtraction was done for the NOMAD data. The diffraction data from NOMAD were used for the Rietveld refinement and the pair distribution function (PDF) analysis. The PDF provides a real-space representation of the local atomic correlations without assuming lattice periodicity. Preferred orientation effects were considered in the Rietveld refinement and were not significant. Single crystal x-ray measurements were carried out using a Bruker D8 Venture single crystal diffractometer (Mo-λ = 0.71 Å) with a Photon III detector and a cryostream that allowed data collection at temperatures between 80 and 500 K. Unit cell refinement and data integration were performed with the Bruker APEX3 software. Single crystal samples were used for the transport measurement and data were collected from 5 to 370 K using Quantum Design Physical Property Measurement System (PPMS). The susceptibility measurements were done under applied magnetic field of $1T$.

Shown in Figs. 1(f) and 1(g) are plots of the temperature dependence of the a- and c-lattice constants from neutron diffraction data collected on warming. The nonmonotonic behavior observed in the thermal expansion of both the a- and c-lattice constants is not typical, with breaks in the slope observed at the CCDW-NCDW and NCDW-ICDW transitions as we see in the transport [Fig. 1(d)]. The discontinuity observed in the a-lattice constant is at or about the CCDW-NCDW transition (between 180 and 300 K). Similarly, in the c-lattice constant, a jump is observed between 180 and 300 K, indicating a negative thermal expansion. The c parameter undergoes sharp decrease at the CDW transition temperatures with a hysteresis behavior that is comparable to the resistivity behavior [48]. On further warming, between 300 and 400 K, the c-lattice constant remains constant with a small drop around 350 K (at the NCDW-ICDW transition), after which it rises with temperature above 400 K in the ICDW phase. The lattice

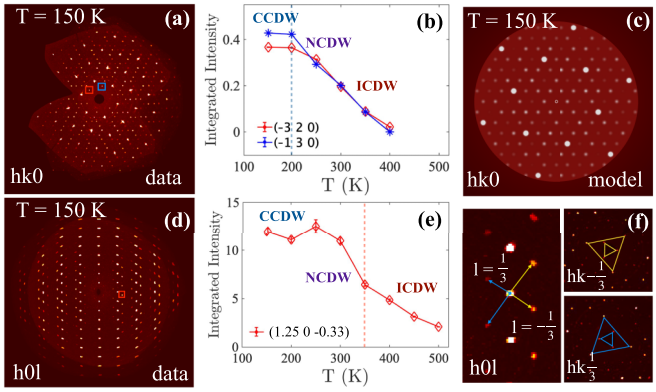

FIG. 2. Single crystal x-ray diffraction precession image of (a) the (hk0) plane and (d) the (0kl) plane in the reciprocal lattice of $1T$-TaS_2 is shown. The weaker supercell reflections, which represent the $\sqrt{13}a\,\sqrt{13}a$ lattice, can be seen in between the bright spots. The data were collected at 150 K. (b) The integrated intensity of superlattice peaks in the (hk0) plane as a function of temperature. (c) The diffraction predicted by the $\sqrt{13}a\,\sqrt{13}a$ superlattice model is shown in the hk0 plane. (e) The integrated intensity of one of the peaks in the (h0l) plane at l=−1/3 as a function of temperature as it undergoes charge density wave transitions. (f) The superlattice reflections along $l = \pm 1/3$ are shown. The data were measured upon warming from 150 to 500 K.

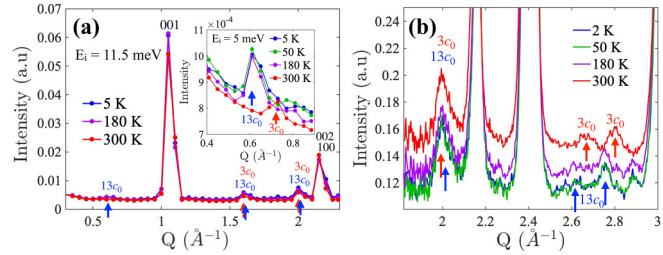

FIG. 3. (a) Powder elastic scans in the low Q region measured at BL-17 at SNS shown as a function of temperature. The satellite peak at $Q \sim 0.62$ Å^{-1} verifying the temperature dependence of $13c$ stacking is shown in the inset. (b) Diffraction data obtained from BL-1B at higher Q showing the temperature dependence of satellite peaks corresponding to CDW modulation and stacking ordering.

constants were obtained from the Rietveld refinement of the diffraction data [Fig. 4(a)]. The data were fit using the low temperature symmetry $P\bar{3}$ that supports the $\sqrt{13}a\,\sqrt{13}a$ superlattice. Several superlattice peaks were observed with the reorientation and expansion of the unit cell from the high temperature phase. The R factor from the refinement is 0.04. Above 300 K, the $P\bar{3}$m1 symmetry fits the data well [3,41].

The periodic lattice distortions in the CDW phase is observed in the x-ray diffraction results on a single crystal of TaS_2. While changes of the stacking order as a function of temperature have been reported in the literature [41,49], there have been no reports on the detailed temperature dependence of the CDW satellite peaks. In this work, we show the temperature evolution of the in-plane and out-of-plane satellite peaks corresponding to the CDW modulation and stacking order. The single crystal x-ray diffraction data were collected on warming from 150 K up to 500 K. In-plane and out-of-plane structural features are mapped to the changes in the resistivity. Precession images collected at 150 K are shown in Fig. 2. At temperatures above the NCDW-ICDW transition, only the primary Bragg peaks from the $P\bar{3}$m1 are visible. Below this transition, in addition to the primary Bragg peaks, superlattice reflections begin to appear. Figure 2(a) is a plot of the hk0-plane in the CCDW phase. The Bragg peaks and superlattice reflections can be reproduced by using the $\sqrt{13}a\,\sqrt{13}a\,\mathrm{R}13.9^0$ structure. The comparison with the simulation shown in Fig. 2(c) is exact (not drawn to scale). The temperature dependence of the integrated intensity of two superlattice reflections in the hk0 plane is plotted in Fig. 2(b). The in-plane $\sqrt{13}a\,\sqrt{13}a\,\mathrm{R}13.9^0$ structure settles below 200 K, at the NCDW-CCDW boundary, and the transition to this phase or out of this phase occurs continuously with temperature. By 400 K, above the NCDW-ICDW transition, the superlattice reflections become indiscernible, indicating that the SODs are either nonexistent or quite diffuse that they do not form a pattern.

Figure 2(d) is a plot of the precession image in the 0kl plane. Here, we observe additional satellites at every Bragg peak at 1/3 that arise from the $3c$ type of ordering in the out-of-plane direction. The satellites in the c direction appear at $l = \pm 1/3$. The temperature dependence of one such peak is shown in Fig. 2(e). Starting from low temperatures, the 1/3 superlattice intensity is steady until the temperature reaches the hysteresis region of the NCDW-ICDW border, at which point the intensity drops. The drop continues through the ICDW transition temperature and gradually disappears by 480 K. Thus, it is clear that the 1/3 satellite exists above 400 K, in the ICDW phase. The $3c$ stacking order persists at 150 K which is slightly below the CCDW transition. Our results suggest that the in-plane and out-of-plane stacking ordering occurs gradually with temperature. Shown in Fig. 2(f) is a plot in the 0kl plane, providing a closer look at the 1/3 peaks. Cuts at constant $l = \pm 1/3$ as in the smaller figures of Fig. 2(f) reproduce the Bragg peaks projected on the hk0 plane.

The temperature dependence of stacking order was investigated further using neutron time-of-flight scattering measurements at low temperatures. Our findings present experimental evidence supporting the existence of two distinct types of stacking order as the material undergoes CCDW to NCDW transition. First, measurements on SEQUOIA of the SNS using an E_i of 11.5 meV showed a satellite peak at $Q \sim 0.62$ Å^{-1} [Fig. 3(a)] at 5 K. The data were integrated along the elastic line only. The peak corresponds to a stacking order of $13c$ as predicted in Refs. [41,49]. This broad peak corresponds to the first order satellites of the $(00l)$ peaks in the CCDW phase with $13c$ stacking order, and is a composite peak corresponding to multiple l values as shown in the Supplemental Material [50]. This peak, as shown in the inset of the figure, disappears upon reaching temperatures above 180 K on warming. Notably, another satellite peak emerges in close proximity to the original peak at 300 K. The additional peak at $Q \sim 0.69$ Å^{-1}, observed at 300 K, corresponding to a $3c$ stacking order [49,51]. The satellite peaks in the low Q region are labeled in Fig. 3 as a signature of $3c$ or $13c$ stacking order. Second, shown in Fig. 3(b) are the low-Q data from

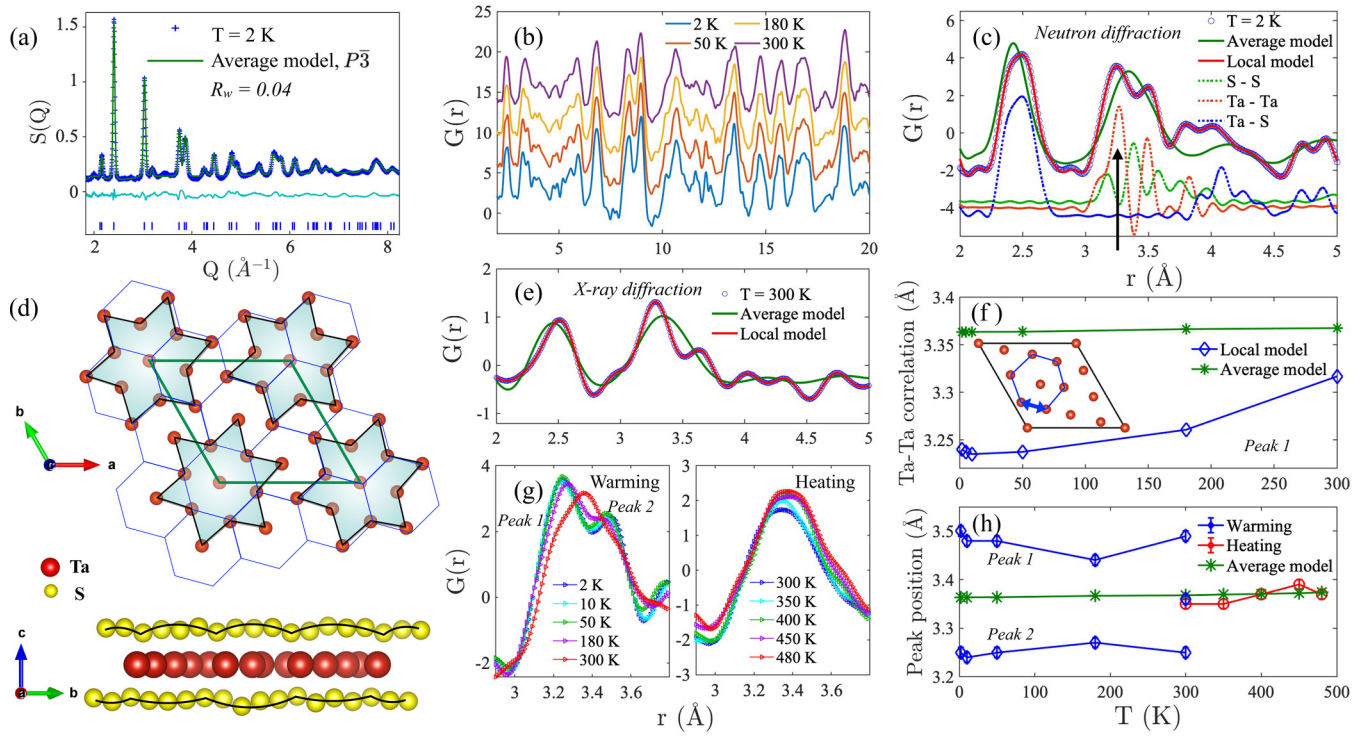

FIG. 4. (a) Structure function determined from neutron diffraction data at 2 K. The data is compared to the $\sqrt{13}a\,\sqrt{13}a$ average model. (b) The experimental neutron PDF as a function of temperature. (c) The experimental neutron PDF data at 2 K compared with the calculated PDF based on the average model and local model. The partial PDFs describing the individual atom pair correlations are shown as well. (d) The in-plane and the out-of-plane local model showing the distorted star of David (SOD) structures within the CCDW superlattice at 2 K. The blue hexagons are shown to represent the Ta atom positions in the absence of any distortions. The Sulfur atoms (yellow spheres) displace away from the symmetry-restricted planes. (e) The experimental x-ray PDF data at 300 K compared with the calculated PDF based on the average and local model. (f) The Ta-Ta correlation corresponding to peak 1, calculated from the local model and average model. The atom pair is shown in the inset. (g) The evolution of the peak around 3.4 Å is shown from 2 to 480 K using the data measured upon (left) warming and (right) heating. The peak splitting is labeled as peak 1 and peak 2, corresponding to the peaks on the left and right, respectively. (h) The position of peak 1 and peak 2 are shown as a function of temperature upon warming and heating. The predicted position based on the average structure is shown for reference.

NOMAD as a function of temperature. Two satellite peaks are observed in the data, at $Q = 1.61$ Å^{-1} and 2.01 Å^{-1} corresponding to first order satellite peaks of $(01l)$. They are present at all temperatures in the measured range from 5 to 300 K. The peak around $Q = 1.62$ Å^{-1} is a composite peak of first order satellites of $(01l)$ and $(10l)$ which are centered at 1.59 Å^{-1}, 1.607 Å^{-1}, and 1.622 Å^{-1} in the $13c$ stacking order (the values are given in Supplemental Tables SII–SIII). On the other hand, in $3c$ stacking, the $Q = 1.62$ Å^{-1} peak corresponds to the first order satellites of (004), $(01l)$, and $(10l)$ in the NCDW phase. There are many such satellites of $3c$ and $13c$ in the higher Q region that are close to each other, but the peak at $Q \sim 0.62$ Å^{-1} is unique and shows a clear temperature dependence of the stacking order at the CCDW-NCDW crossover. Thus we conclude that when the structure is cooled all the way down to 5 K, the $13c$ stacking forms and is stable up to the CCDW-NCDW crossover temperature around 180 K. Above this temperature, the $13c$ order disappears and we see evidence of $3c$ stacking. Details on predicted peak positions and a comparison with data at 2 and 300 K are shown in Tables S II and S III [50].

On further probing the atomic structure to investigate how the CDW modulations are evident in the local atomic correlations, we observed a local structural anomaly that is coupled to the hysteresis observed in the resistivity. The neutron powder diffraction data collected at NOMAD of the SNS [shown in Fig. 4(a)] and x-ray powder diffraction data collected at 11-ID-C of the APS were Fourier transformed to obtain the pair distribution function (PDF). Probing the local structure with x-rays and neutrons provided constraints to the real-space model that enabled a detailed picture of the changes emerging with the phase transitions. Previous x-ray PDF studies confirmed the presence of SOD formation [52], however, we report the anomalous distortions within the star clusters and quantify the temperature dependence of such distortions from 2 to 480 K. The $G(r)$'s as a function of temperature denoting the atom pair correlations are shown in Fig. 4(b). The notable differences in PDF arises at lower r region, and we do not see any discernible changes in $G(r)$ at higher r range. Changes are observed as a function of temperature, which we elaborate on next. Shown in Fig. 4(c) is a plot of the neutron G(r) determined at 2 K and compared to a model calculated using the atomic coordinates and unit cell dimensions of $\sqrt{13}a\,\sqrt{13}a$ superlattice structure. We call this the "average model" as it is based on the symmetry that describes the periodic unit cell. It is evident, however, that the

periodic lattice of the $\sqrt{13}a\,\sqrt{13}a$ alone does not adequately describe the local atomic structure [Fig. 4(c)]. Differences are observed between the two, and the discrepancy around 3 to 4.5 Å is the most striking. The discrepancy is also evident in the x-ray $G(r)$ data of Fig. 4(e) at 300 K. A better fit to the local structure is obtained by allowing Ta and S atoms displacements leading to the distortions shown in Fig. 4(d). In-plane SOD arrangements are distorted away from the ideal hexagonal geometry, while out-of-plane S distortions lead to a modulation that runs parallel to the plane. Figure 4(f) is a plot of the local Ta-Ta correlations at ∼3.3 Å obtained from the fitting of the $G(r)$ data compared to the Ta-Ta bond obtained from the average structure [see inset of Fig. 4(f)]. This Ta-Ta correlation is indicated by a black arrow in the partial PDF shown in Fig. 4(c). While the particular Ta-Ta bond does not change with temperature in the average structure, locally, it is shorter and changes with temperature, as shown in Fig. 4(f).

Also shown in Figs. 4(c) and 4(e) at 2 K (CCDW) and 300 K (NCDW), respectively, is a comparison of the calculated $G(r)$ based on the local model of Fig. 4(d). The agreement is very good. In this model, the SODs are faulty in real space, where the Ta atoms move within the plane and locally break the $P\bar{3}$ symmetry. The Ta distortions are continuous as a function of temperature, with the maximum atom displacements observed at 2 K [Fig. 4(f)]. The hexagonal lattice shown in the background of the stars corresponds to the average symmetry of $P\bar{3}$. Thus it is clear that the symmetry-breaking local distortions occur, but such distortions are not sufficient to break the long-range symmetry because the distortions average out in all orientations in the crystal. Also shown in this figure are the out-of-plane S distortions where a quasiperiodic modulation propagates in the direction tangential to the c axis.

Shown in Fig. 4(g) is the temperature dependence of the $G(r)$ in a narrow range between 3 and 3.8 Å, with the two peaks identified as Peak 1 and Peak 2. The left panel is for data collected on warming after the sample was cooled all the way down to 2 K. The right panel shows data collected on heating above 300 K. From the partial plots of Fig. 4(c), it can be seen that Ta-Ta and S-S pair correlations contribute to the total PDF in this region. The temperature dependence of peaks 1 and 2 are shown in Fig. 4(h). The peak splitting primarily arises from the local Ta-Ta correlations and secondly from S-S correlations. In comparison to the average model, where only one broad correlation peak is observed in that region at all temperatures, the real space correlations are split, and the split changes with temperature. For data collected on warming, it is clear that the faulty arrangement of the stars is retained through the NCDW transition. For data collected on heating from 300 K, there is no memory of the faulty stars and only one broad correlation is observed. At 300 K, the data on warming and heating is different because of the structural hysteresis. Thus the resistivity behavior on warming is most likely associated with structural hysteresis. Stacking of the CDW ordered planes plays a key role in the formation of the gap at the Fermi level [17]. It has been theoretically proposed that hybridization of the d_{z^2} orbitals along c can lead to a gap at the Γ point. The temperature dependence of the local distortions, formation of the superlattice, and out-of-plane stacking order provide evidence for strong electron-lattice coupling that may hold the key to the gap opening in the density of states. Moreover, the band-filling scenario is not consistent with our observations because of the presence of distortions. Instead, a more likely scenario must involve electron-phonon and electron-electron correlations.

This work has been supported by National Science Foundation Grant No. 2219493. The authors acknowledge Yang Ren for assistance provided with the 11-ID-C measurement, and Jianshi Zhou for help with the magnetic susceptibility measurement. A portion of this research used resources at the Spallation Neutron Source, a DOE Office of Science User Facility operated by Oak Ridge National Laboratory. Use of the Advanced Photon Source at Argonne National Laboratory, Office of Science user facility, was supported by the U.S. Department of Energy, Office of Science, Office of Basic Energy Sciences. Single-crystal x-ray diffraction experiments were performed on a diffractometer at the University of Virginia, which is funded by the NSF-MRI program (Grant No. CHE-2018870).

[1] G Gruner, *Density Waves in Solids* (Addison-Wesley, Boston, 1994).

[2] J. A. Wilson, F. J. Di Salvo, and S. Mahajan,Charge-Density Waves in Metallic, Layered, Transition-Metal Dichalcogenides, Phys. Rev. Lett. **32**, 882 (1974).

[3] J. A. Wilson, F. J. Di Salvo, and S. Mahajan, Charge-density waves and superlattices in the metallic layered transition metal dichalcogenides, Adv. Phys. **24**, 117 (1975).

[4] W. Choi, N. Choudhary, G. H. Han, J. Park, D. Akinwande, and Y. H. Lee, Recent development of two-dimensional transition metal dichalcogenides and their applications, Mater. Today **20**, 116 (2017).

[5] M. Kang, B. Kim, S. H. Ryu, S. W. Jung, J. Kim, L. Moreschini, C. Jozwiak, E. Rotenberg, A. Bostwick, and K. S. Kim, Universal mechanism of band-gap engineering in transition-metal dichalcogenides, Nano Lett. **17**, 1610 (2017).

[6] S. Manzeli, D. Ovchinnikov, D. Pasquier, O. V. Yazyev, and A. Kis, 2d transition metal dichalcogenides, Nat. Rev. Mater. **2**, 17033 (2017).

[7] X. Zhu, J. Guo, J. Zhang, and E. W. Plummer, Misconceptions associated with the origin of charge density waves, Adv. Phys. X **2**, 622 (2017).

[8] P. Chen, W. W. Pai, Y.-H. Chan, A. Takayama, C.-Z. Xu, A. Karn, S. Hasegawa, M.-Y. Chou, S.-K. Mo, A.-V. Fedorov *et al.*, Emergence of charge density waves and a pseudogap in single-layer $TiTe_2$, Nat. Commun. **8**, 516 (2017).

[9] R. H. Friend and D. Jérome, Periodic lattice distortions and charge density waves in one-and two-dimensional metals, J. Phys. C **12**, 1441 (1979).

[10] P. Fazekas and E. Tosatti, Electrical, structural and magnetic properties of pure and doped $1T$-TaS_2, Philos. Mag. B **39**, 229 (1979).

[11] J. C. Petersen, S. Kaiser, N. Dean, A. Simoncig, H. Y. Liu, A. L. Cavalieri, C. Cacho, I. C. E. Turcu, E. Springate, F. Frassetto, L. Poletto, S. S. Dhesi, H. Berger, and A. Cavalleri, Clocking the Melting Transition of Charge and Lattice Order in $1T$-TaS_2 with Ultrafast Extreme-Ultraviolet Angle-Resolved Photoemission Spectroscopy, Phys. Rev. Lett. **107**, 177402 (2011).

[12] S. Hellmann, M. Beye, C. Sohrt, T. Rohwer, F. Sorgenfrei, H. Redlin, M. Kallane, M. Marczynski-Buhlow, F. Hennies, M. Bauer, A. Fohlisch, L. Kipp, W. Wurth, and K. Rossnagel, Ultrafast Melting of a Charge-Density Wave in the Mott Insulator $1T$-TaS_2, Phys. Rev. Lett. **105**, 187401 (2010).

[13] R. E. Thomson, B. Burk, A. Zettl, and J. Clarke, Scanning tunneling microscopy of the charge-density-wave structure in $1T$-TaS_2, Phys. Rev. B **49**, 16899 (1994).

[14] C. J. Butler, M. Yoshida, T. Hanaguri, and Y. Iwasa, Mottness versus unit-cell doubling as the driver of the insulating state in $1T$-TaS_2, Nat. Commun. **11**, 2477 (2020).

[15] Y. D. Wang, W. L. Yao, Z. M. Xin, T. T. Han, Z. G. Wang, L. Chen, C. Cai, Y. Li, and Y. Zhang, Band insulator to Mott insulator transition in $1T$-TaS_2, Nat. Commun. **11**, 4215 (2020).

[16] T. Ritschel, J. Trinckauf, K. Koepernik, B. Büchner, M. v. Zimmermann, H. Berger, Y. I. Joe, P. Abbamonte, and J. Geck, Orbital textures and charge density waves in transition metal dichalcogenides, Nat. Phys. **11**, 328 (2015).

[17] T. Ritschel, H. Berger, and J. Geck, Stacking-driven gap formation in layered $1T$-TaS_2, Phys. Rev. B **98**, 195134 (2018).

[18] S.-H. Lee, J. S. Goh, and D. Cho, Origin of the Insulating Phase and First-Order Metal-Insulator Transition in $1T$-TaS_2, Phys. Rev. Lett. **122**, 106404 (2019).

[19] L. Chaix, G. Ghiringhelli, Y. Y. Peng, M. Hashimoto, B. Moritz, K. Kummer, N. B. Brookes, Y. He, S. Chen, S. Ishida *et al.*, Dispersive charge density wave excitations in $Bi_2SrCaCu_2O_{8+\delta}$, Nat. Phys. **13**, 952 (2017).

[20] E. Dagotto, Complexity in strongly correlated electronic systems, Science **309**, 257 (2005).

[21] X. M. Chen, C. Mazzoli, Y. Cao, V. Thampy, A. M. Barbour, W. Hu, M. Lu, T. A. Assefa, H. Miao, G. Fabbris *et al.*, Charge density wave memory in a cuprate superconductor, Nat. Commun. **10**, 1435 (2019).

[22] J. M. Tranquada, B. J. Sternlieb, J. D. Axe, Y. Nakamura, and S.-i. Uchida, Evidence for stripe correlations of spins and holes in copper oxide superconductors, Nature (London) **375**, 561 (1995).

[23] J. M. Tranquada, J. D. Axe, N. Ichikawa, A. R. Moodenbaugh, Y. Nakamura, and S. Uchida, Coexistence of, and Competition Between, Superconductivity and Charge-stripe Order in $La_{1.6-x}Nd_{0.4}Sr_xCuO_4$, Phys. Rev. Lett. **78**, 338 (1997).

[24] S. A. Kivelson, I. P. Bindloss, E. Fradkin, V. Oganesyan, J. M. Tranquada, A. Kapitulnik, and C. Howald, How to detect fluctuating stripes in the high-temperature superconductors, Rev. Mod. Phys. **75**, 1201 (2003).

[25] J. M. Tranquada, H. Woo, T. G. Perring, H. Goka, G. D. Gu, G. Xu, M. Fujita, and K. Yamada, Quantum magnetic excitations from stripes in copper oxide superconductors, Nature (London) **429**, 534 (2004).

[26] L. Balents, Spin liquids in frustrated magnets, Nature (London) **464**, 199 (2010).

[27] K. T. Law and P. A. Lee, $1T$-TaS_2 as a quantum spin liquid, Proc. Natl. Acad. Sci. **114**, 6996 (2017).

[28] P. W. Anderson, Resonating valence bonds: A new kind of insulator? Mater. Res. Bull. **8**, 153 (1973).

[29] P. W. Anderson, The resonating valence bond state in La_2CuO_4 and superconductivity, Science **235**, 1196 (1987).

[30] T.-H. Han, J. S. Helton, S. Chu, D. G. Nocera, J. A. Rodriguez-Rivera, C. Broholm, and Y. S. Lee, Fractionalized excitations in the spin-liquid state of a kagome-lattice antiferromagnet, Nature (London) **492**, 406 (2012).

[31] Y. Zhou, K. Kanoda, and T.-K. Ng, Quantum spin liquid states, Rev. Mod. Phys. **89**, 025003 (2017).

[32] K. E. Wagner, E. Morosan, Y. S. Hor, J. Tao, Y. Zhu, T. Sanders, T. M. McQueen, H. W. Zandbergen, A. J. Williams, D. V. West, and R. J. Cava, Tuning the charge density wave and superconductivity in Cu_xTaS_2, Phys. Rev. B **78**, 104520 (2008).

[33] X.-Y. Zhu, S. Wang, Z.-Y. Jia, L. Zhu, Q.-Y. Li, W.-M. Zhao, C.-L. Xue, Y.-J. Xu, Z. Ma, J. Wen, S. L. Yu, J. X. Li, and S. C Li, Realization of a Metallic State in $1T$-TaS_2 with Persisting Long-range Order of a Charge Density Wave, Phys. Rev. Lett. **123**, 206405 (2019).

[34] Y. Ma, Y. Hou, C. Lu, L. Li, and C. Petrovic, Possible origin of nonlinear conductivity and large dielectric constant in the commensurate charge-density-wave phase of $1T$-TaS_2, Phys. Rev. B **97**, 195117 (2018).

[35] H. Li, T. T. Zhang, A. Said, G. Fabbris, D. G. Mazzone, J. Q. Yan, D. Mandrus, G. B. Halász, S. Okamoto, S. Murakami *et al.*, Giant phonon anomalies in the proximate Kitaev quantum spin liquid α-$RuCl_3$, Nat. Commun. **12**, 3513 (2021).

[36] L. V. Gasparov, K. G. Brown, A. C. Wint, D. B. Tanner, H. Berger, G. Margaritondo, R. Gaál, and L. Forró, Phonon anomaly at the charge ordering transition in $1T$-TaS_2, Phys. Rev. B **66**, 094301 (2002).

[37] K. S. Novoselov, D. Jiang, F. Schedin, T. J. Booth, V. V. Khotkevich, S. V. Morozov, and A. K. Geim, Two-dimensional atomic crystals, Proc. Natl. Acad. Sci. **102**, 10451 (2005).

[38] J. R. Schaibley, H. Yu, G. Clark, P. Rivera, J. S. Ross, K. L. Seyler, W. Yao, and X. Xu, Valleytronics in 2D materials, Nat. Rev. Mater. **1**, 16055 (2016).

[39] T. Mueller, TMDs–optoelectronic devices, in *2D Materials* (Cambridge University Press, Cambridge, 2017), pp. 329–343.

[40] O. M. J. Van't Erve, A. T. Hanbicki, A. L. Friedman, K. M. McCreary, E. Cobas, C. H. Li, J. T. Robinson, and B. T. Jonker, Graphene and monolayer transition-metal dichalcogenides: properties and devices, J. Mater. Res. **31**, 845 (2016).

[41] C. B. Scruby, P. M. Williams, and G. S. Parry, The role of charge density waves in structural transformations of $1T$ TaS_2, Philos. Mag. **31**, 255 (1975).

[42] B. Sipos, A. F. Kusmartseva, A. Akrap, H. Berger, L. Forró, and E. Tutiš, From Mott state to superconductivity in $1T$-TaS_2, Nat. Mater. **7**, 960 (2008).

[43] Q. Dong, Q. Li, S. Li, X. Shi, S. Niu, S. Liu, R. Liu, B. Liu, X. Luo, J. Si *et al.*, Structural phase transition and superconductivity hierarchy in $1T$-TaS_2 under pressure up to 100 GPa, npj Quantum Mater. **6**, 20 (2021).

[44] Y. Liu, R. Ang, W. J. Lu, W. H. Song, L. J. Li, and Y. P. Sun, Superconductivity induced by Se-doping in layered charge-density-wave system $1T$-$TaS_{2-x}Se_x$, Appl. Phys. Lett. **102**, 192602 (2013).

[45] T. Pillo, J. Hayoz, H. Berger, M. Grioni, L. Schlapbach, and P. Aebi, Remnant Fermi Surface in the Presence of an Underlying

Instability in Layered $1T$-TaS_2, Phys. Rev. Lett. **83**, 3494 (1999).

[46] R. Brouwer, *Incommensurability in Crystal Structures* (University of Groningen, Groningen, 1978).

[47] K. Rossnagel, On the origin of charge-density waves in select layered transition-metal dichalcogenides, J. Phys.: Condens. Matter **23**, 213001 (2011).

[48] F. L. Givens and G. E. Fredericks, Thermal expansion op $NbSe_2$ and TaS_2, J. Phys. Chem. Solids **38**, 1363 (1977).

[49] A. Spijkerman, J. L. de Boer, A. Meetsma, G. A. Wiegers, and S. van Smaalen, X-ray crystal-structure refinement of the nearly commensurate phase of $1T$-TaS_2 in (3+2)-dimensional superspace, Phys. Rev. B **56**, 13757 (1997).

[50] See Supplemental Material at http://link.aps.org/supplemental/10.1103/PhysRevB.107.184109 for more detailed analysis and plots.

[51] P. M. Williams, G. S. Parry, and C. B. Scrub, Diffraction evidence for the Kohn anomaly in $1T$ TaS_2, Philos. Mag. **29**, 695 (1974).

[52] V. Petkov, J. E. Peralta, B. Aoun, and Y. Ren, Atomic structure and Mott nature of the insulating charge density wave phase of $1T$-TaS_2, J. Phys.: Condens. Matter **34**, 345401 (2022).